

Dielectric relaxations of nanocomposites composed of HEUR polymers and magnetite nanoparticles

A. Campanella^{1*}, A. Brás², K. N. Raftopoulos³, C. M. Papadakis³, O. Vassiliadou⁴, A. Kyritsis⁴,
M. S. Appavou¹, P. Müller-Buschbaum³, H. Frielinghaus¹

¹ JCNS, Forschungszentrum Jülich GmbH, outstation at FRMII, Lichtenbergstrasse 1, 85747 Garching, Germany

² Universität zu Köln, Institut für Physikalische Chemie, Luxemburger Str. 116, 50939 Köln, Germany

³ Technische Universität München, Physik-Department, Lehrstuhl für Funktionelle Materialien/Fachgebiet Physik weicher Materie, James-Franck-Straße 1, 85748 Garching, Germany

⁴ National Technical University of Athens, Physics Department, Iroon Polytechniou 9, Zografou Campus, Athens, 15780, Greece

*Corresponding author, a.campanella@fz-juelich.de, +49089 289 10774

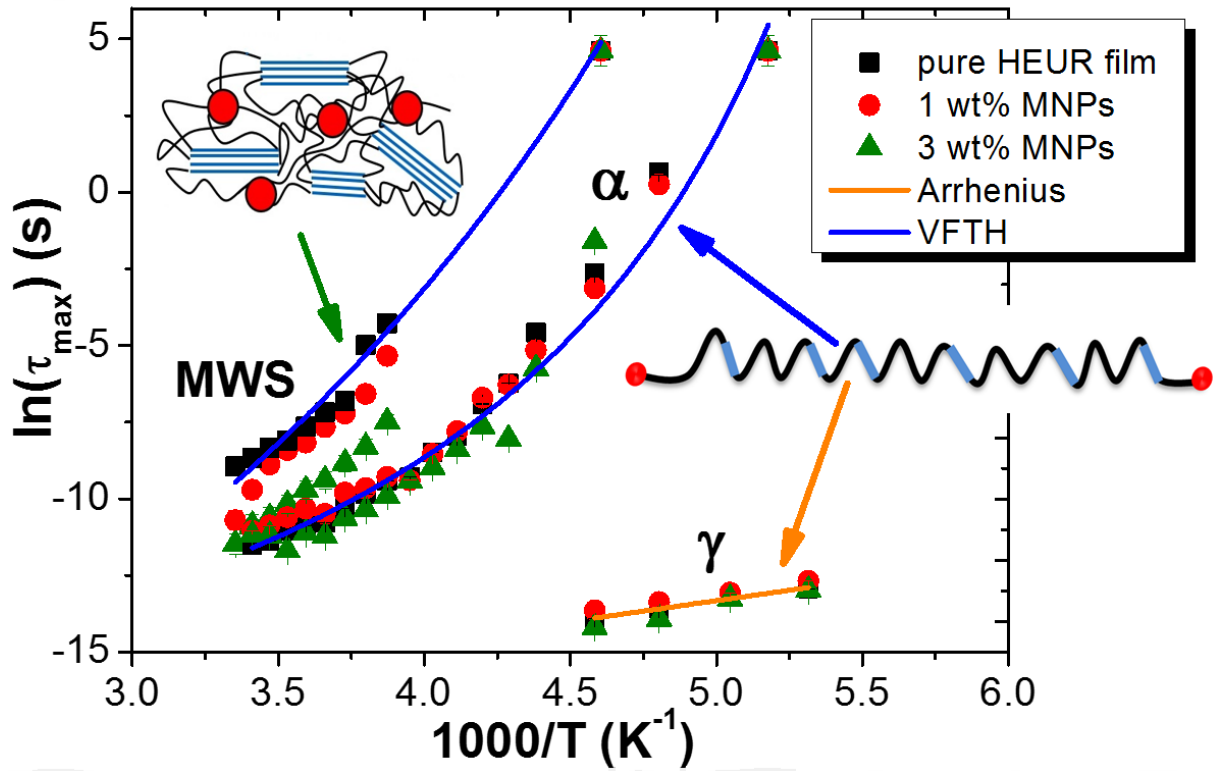
Abstract

We investigate the dynamics of nanocomposites composed of hydrophobically modified ethoxylated urethanes (HEUR) and magnetite nanoparticles (MNPs) as dry films. We employed dielectric relaxation spectroscopy (DRS) in combination with differential scanning calorimetry (DSC) and thermally stimulated depolarization currents (TSDC). The three techniques reveal a strong heterogeneity of the matrix of the nanocomposites, consisting of (i) a crystalline poly(ethyleneoxide) PEO bulk phase, (ii) an amorphous PEO portion, and (iii) small PEO crystallites which experience different constraints than the PEO bulk phase. TSDC and DRS reveal a very high direct current (DC)-conductivity

of the pure matrix, which increases with MNPs concentration. The increase of the DC-conductivity is not related to an increase of the segmental mobility, but most likely to the change of the morphology of the hydrophobic domains of the polymer matrix, due to the formation of large MNPs clusters. Indeed, the MNPs neither influence the segmental dynamics of the polymer nor the phase behavior of the polymer matrix. The addition of MNPs slightly increases the activation energy related to the γ -relaxation of the polymer. This effect might be related to the changes in nano-morphology as demonstrated by the slight increase of the degree of crystallinity. The analysis of the DRS data with the electrical modulus $M''(\omega)$ and the derivative ε''_{der} formalism allow us to identify a low-frequency process in addition to the conductivity relaxation. This low-frequency dispersion is also revealed by TSDC. It is most likely related to the Maxwell-Wagner-Sillars relaxation, which typically occurs in systems which feature phase separation. The detailed investigation of the dielectric properties of these novel nanocomposites with increasing MNPs concentration will be useful for their practical application, for example as absorbers of electromagnetic waves.

(Keywords: nanocomposites, magnetite nanoparticles, dynamics, heterogeneity, conductivity)

Graphical abstract



1. Introduction

The combination of magnetic and dielectric properties, the stability and the biocompatibility make magnetic nanocomposite materials suitable for both, environmental and biomedical applications and for use in electronics [1-6]. Typically, the magnetic nanocomposite materials comprise a polymer matrix and inorganic filler particles. The polymer matrix is used for processing, whereas the inorganic filler adds the magnetic contribution to the system. In particular, nanocomposites containing magnetite (Fe_3O_4) nanoparticles as fillers show interesting microwave absorbing properties, for instance [7, 8]. To disperse the magnetic nanoparticles in the polymer matrix, miscibility is required, which typically can be achieved by coating the nanoparticles [9, 10]. By using special polymers, such as diblock copolymers, the polymer matrix can be used as a

template to guide the nanoparticles, which can give rise to special magnetic properties [11-15]. However, for large-scale applications the use of tailor-made diblock copolymers may be expensive and consequently disadvantageous. Statistical copolymers or other structures polymers may also be able to embed magnetic nanoparticles selectively [16] and are more readily available.

In this work, we present a magnetic nanocomposite system based on hydrophobically modified ethoxylated urethanes (HEUR) with embedded coated magnetite (Fe_3O_4) nanoparticles (**Fig. 1**). As shown in **Fig. 1 b**), the MNPs are coated with both surfactants oleic acid and oleylamine, since it ensure a high stabilization of the MNPs dispersion [17]. The choice of polyurethanes as polymer matrices has advantages in terms of versatility, since they can behave as elastomers, thermoplastics or thermoset polymers [18]. Furthermore, the presence of alkyl end-groups in the polymer structure allows a hydrophobic interaction with the hydrophobically coated magnetic nanoparticles (MNPs) and eventually to their homogeneous dispersion. These features widen the applicability of the final nanocomposite. The structural characterization of these novel nanocomposites by small angle neutron scattering (SANS) was presented in our previous study [16]. In this preceding work, we observed a microphase separation of the polymer matrix into hydrophobic end-chains and into the hydrophilic backbone of the telechelic HEUR polymer. Note that this type of microphase separation differs qualitatively from that observed in conventional polyurethanes, where the so-called hard domains, which contain the urethane groups, separate from the soft flexible matrix due to the hydrogen bonding between the urethane groups. Furthermore, for MNPs concentrations above 0.8 wt%, the formation of dense MNPs clusters was observed. Following this structural characterization of the HEUR-MNPs nanocomposites, in the present study, we focus on the dynamics of the system. At this, we employed dielectric relaxation spectroscopy

(DRS), which is a powerful tool for studying the polymer dynamics in a broad temperature and frequency range [19]. Along with the conventional alternating current (AC)-dielectric spectroscopy, we employed the technique of thermally stimulated depolarization current (TSDC). TSDC is a special dielectric technique in the temperature domain, which extends the range of relaxation times up to approximately 100 s, a value which is typically not accessible by conventional AC techniques. The results from the dielectric measurements are compared with the ones from differential scanning calorimetry (DSC). In order to clarify the origin of some of the phase transitions observed in the DSC measurements, we carried out water sorption measurements in order to quantify the water content in the dry films. We relate the dielectric behavior to the morphology of the system and determine the relation of the polymer dynamics to the MNP concentration. By combining DSC, TSDC and DRS, we observe a very strong heterogeneity of the PEO portion of polymer matrix of the nanocomposites. The dynamics of the system is not affected by the MNP concentration, and only an increase of the direct current (DC)-conductivity is observed with MNP concentration, which may be related to the increase of the charge carriers in the system.

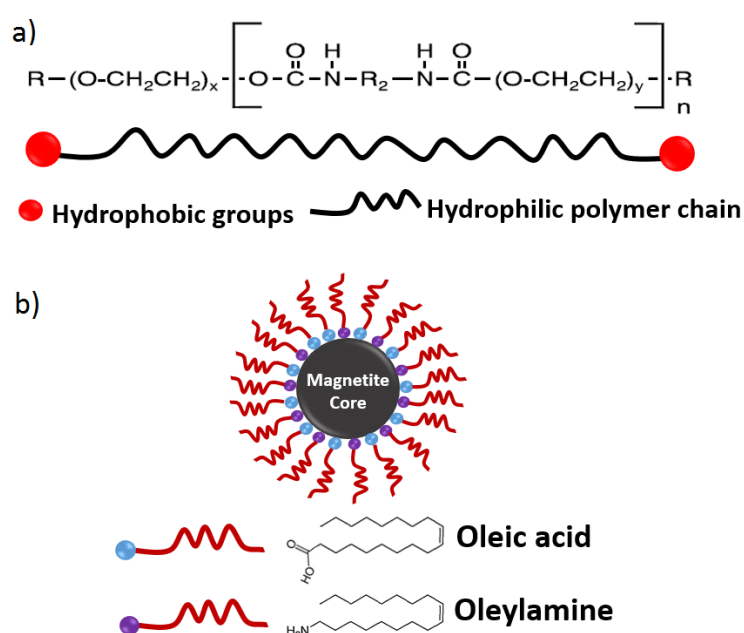


Fig. 1 a) Chemical structure and sketch of the HEUR polymer ($n = 10$, $y = 16$, $R_2 = C_4H_8$, $R=C_{22}H_{44}$). **b)** Sketch of the magnetite nanoparticles coated with oleic acid and oleylamine

2. Experimental

2.1 Materials

The telechelic polymer is the commercial TAFIGEL PUR 61 (25% water emulsion, $M_w = 8900$ g/mol, $D = 1.04$) and was purchased from Münzing Chemie GmbH (Heilbronn, Germany). For the synthesis of the hydrophobic MNPs, iron (III) acetylacetonate ($Fe(acac)_3$, 99.9%), 1,2 hexadecanediol ($C_{14}H_{29}CH(OH)CH_2(OH)$, 90%), oleylamine (OAM, $C_{18}H_{33}NH_2$, 70%), oleic acid (OA, $C_{18}H_{33}COOH$, 99%) phenylether ($C_{12}H_{10}O$, 99%), and solvents (hexane, ethanol) were purchased from Sigma Aldrich. The synthesis of the magnetite nanoparticles coated with oleic acid and oleylamine was carried out by thermal decomposition of iron Fe(III) salt according to the procedure reported by Wang et al [17].

2.2 Nanocomposites preparation

The preparation of the nanocomposites in the dried state was performed following the procedure described in our previous work [16]. They were obtained by casting a solution of polymers and nanoparticles in a mixture of H_2O and hexane onto a solid support and by evaporating the solvent. A metallic frame with a depth of 1 mm was used as a support for the casting. More precisely, a mixture of 0.74 g of the polymer solution in water (25 wt %) and 0.8 mL of a stock solution of a 2.3 g/L solution of the MNPs in hexane was carefully spread on the metallic support. Then, the solvent was evaporated for 48 h at room

temperature. The resulting nanocomposite had a MNP concentration of 1 wt %. We prepared the nanocomposite having 3 wt% MNP concentration following the same procedure. The pure HEUR film was obtained by solution casting from a 25 wt% solution of HEUR polymer in H₂O. We obtained films having thicknesses of the order of 1 mm.

2.3 Water sorption measurements

Water sorption measurements were performed at 25 °C on the pure HEUR film and on the HEUR nanocomposites with 1 wt% and 3 wt% MNP concentration. A TA Instruments VTI-SA Vapor Sorption Analyzer was used. For the pure HEUR film, during sorption, saturation was achieved for relative humidities rh between 5 % and 80 %. For $rh > 80$ %, the sample mass continued to increase without saturating, indicating that the sample started to dissolve. Due to this behavior, the water desorption was only monitored for 85% rh , again without reaching saturation. For the nanocomposite with 3 wt% MNPs, the desorption process was monitored over the whole range of relative humidities explored, and the measurement revealed that no hysteresis occurs for $rh \leq 80\%$.

2.4 Differential Scanning Calorimetry (DSC)

The glass transition and crystallization/melting events were investigated in nitrogen atmosphere in the temperature range from -150 °C to 150 °C by a TA Instruments Q200 differential scanning calorimeter. A few mg of sample were placed in aluminum T₀ pans (by TA Instruments). Three cooling scans were performed with starting temperatures of 150°C, 80 °C and 40 °C down to -150 °C, and two heating scans from -150 °C up to 80 °C and 90 °C with 10 °C/min.

2.5 Thermally stimulated depolarization currents (TSDC)

TSDC is a dielectric technique in the temperature domain, which roughly corresponds to measuring the dielectric loss as a function of temperature at a fixed low frequency in the range 10^{-4} - 10^{-2} Hz (equivalent frequency) [20]. The sample was inserted between the plates of a parallel capacitor and was polarized by an electric field E_p at a polarizing temperature T_p for a time t_p . With the electric field still applied, the sample was cooled to a temperature T_o , which is chosen to be low enough to prevent depolarization by thermal energy. Then, the sample was short-circuited and reheated at a constant rate b . The discharge current generated during heating was measured as a function of temperature with a sensitive electrometer. TSDC measurements were carried out in the temperature range from -150 to 20 °C using a Keithley 617 electrometer in combination with a Novocontrol sample cell for TSDC measurements. Typical experimental conditions were $T_p = 20$ °C or -60°C, $E_p = 5$ kV/cm, $t_p = 5$ min, a cooling rate of 10 K/min, $T_o = -150$ °C, and $b = 3$ K/min.

2.6 Dielectric relaxation spectroscopy (DRS)

The matrix and the two nanocomposites (with 1 and 3 wt% of MNPs) were investigated by dielectric spectroscopy using a Novocontrol Impedance Spectrometer (Novocontrol Technologies GmbH & Co. KG Montabaur, Germany) in the frequency range 0.01 Hz-1 MHz and in the temperature range from 25 °C to -85 °C in steps of 5 °C or of 10 °C. The measurements were performed during cooling. A film of each sample (1 mm) was placed between two gold plated electrodes (diameter 20 mm) of a parallel plate capacitor. The

sample was mounted in a cryostat, and the temperature was controlled by a heated gas stream of nitrogen, evaporated from the liquid state. The temperature was controlled by a nitrogen jet (Quatro, Novocontrol), with an uncertainty of 0.1 °C during every frequency sweep.

2.7 Transmission electron microscopy measurements

The nanocomposites in the dried state were investigated with Transmission electron microscopy (TEM) in order to obtain the shape and the size distribution of the MNPs. The samples were prepared by depositing the powder sample on a carbon-coated copper grid. After a few minutes, excess powder was carefully removed. The specimen was inserted into a high-tilt-specimen retainer (EM-21311HTR, JEOL, Tokyo, Japan) and transferred to a JEM 2200 FS EFTEM instrument (JEOL, Tokyo, Japan). Examinations were carried out at room temperature. The transmission electron microscope was operated at an acceleration voltage of 200 kV. Zero-loss filtered images were recorded digitally by a bottom-mounted 16 bit CCD camera system (FastScan F214, TVIPS, Munich, Germany). Images (**Fig.15**) were taken with EMenu 4.0 image acquisition program (TVIPS, Munich, Germany).

3. Results and discussion

3.1 Determination of the water content: water sorption measurements

In order to characterize the presence of water in the polymer matrix of the dry films, the water content in the HEUR polymer film and in the nanocomposites was quantified by water sorption measurements. The confirmation of the presence of the water trapped in the

prepared films and its quantification is important to understand the thermal and dielectric behavior of the investigated systems. In **Fig. 2**, the evolution of the sample mass (pure HEUR film) with time during the water sorption process is shown. The step-like increase of the sample mass is due to the water uptake during the water sorption process. For relative humidities rh between 5 % and 80 %, the mass vs time profiles reach a plateau within 2 h, i.e. they reach saturation within this time (green arrow in **Fig. 2**). For rh higher than 80 %, saturation is not reached, which is due to the fact that the sample starts to dissolve (blue arrow in **Fig. 2**).

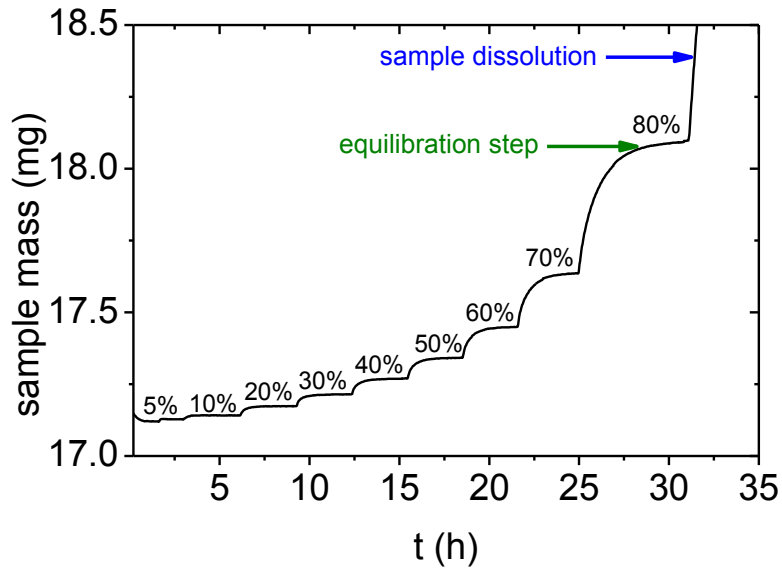


Fig. 2 Mass of the pure HEUR film as a function of the time at different relative humidity values rh , as indicated in the graph

The sorption isotherm at 25 °C for the pure HEUR film is shown in **Fig. 3**. It shows the water content as a function of the water activity a_w or relative humidity rh .

The water content h_d is defined as:

$$h_d = \frac{m_w}{m_d} \quad (1)$$

where m_w is the mass of the absorbed water and m_d the mass of the dry sample. In the present case, the mass of the dry sample refers to the mass of the sample after vacuum drying at room temperature for 24 h.

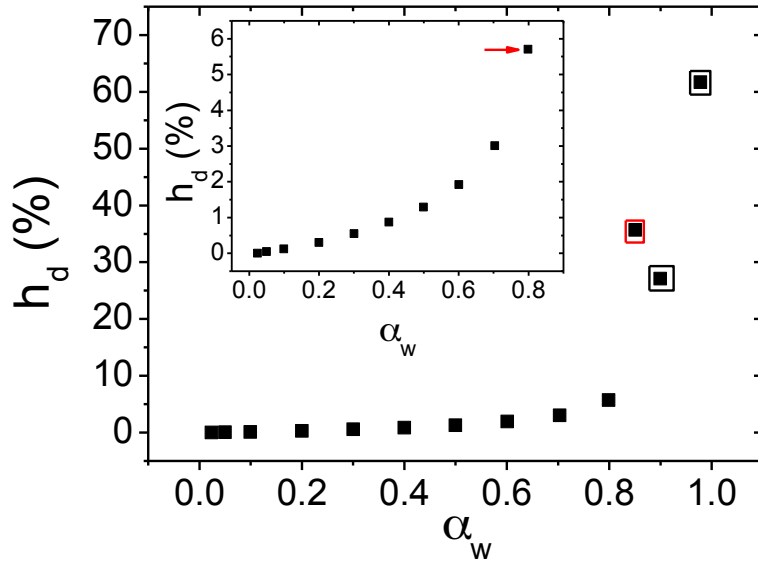


Fig. 3 Water content h_d (%) in the pure HEUR film as a function of the water activity α_w . The inset graph is the sorption isotherm for the equilibrated steps. The red arrow highlights the water content at 80 % rh , the highest value where equilibrium is reached. The data points surrounded by black squares are the ones acquired out of equilibration during the sorption process, and the one marked by the red square was acquired during the desorption process.

The data points marked by black squares are the ones which are out of equilibration during the sorption process, and the one marked by the red square is measured during the water desorption process. The sample absorbs up to 6% of water at $\alpha_w = 0.8$ (relative humidity $rh = 80\%$). Furthermore, the water content h_d vs the water activity α_w does not show a linear behavior for $\alpha_w > 0.6$. This behavior is typical of hydrogel systems and is due to the formation of clusters of water molecules [21]. Therefore, we can state that in usual

conditions, i.e. in a relative humidity range rh of 40% and 80%, the pure HEUR film has a water content, h_d , between 1% and 6%.

The water sorption measurements on the nanocomposites (the data of the nanocomposite with 3 wt% MNPs are shown in **Fig. S1** in the SI) monitoring both, the sorption and the desorption process, imply that no hysteresis is observed for a relative humidity below 85%. In this case, the nanocomposite absorbs up to 6 % of water at $\alpha_w = 0.8$ (relative humidity $rh = 80\%$), as for the pure HEUR film, meaning that the presence of the MNPs does not influence the water uptake of the polymer matrix. The presence of water in all the investigated samples has to be taken into account in the investigation of their thermal behavior and in the interpretation of their dielectric relaxation spectra.

3.2 Thermal behavior: Differential scanning calorimetry (DSC)

The phase transitions of the pure HEUR polymer film and the nanocomposites with MNP concentrations of 1 wt% and 3 wt% were followed using DSC. The DSC curves of all samples feature the same phase transitions at the same temperatures. Therefore, for clarity, in **Fig. 4**, the whole DSC curve (heating scans on the top and cooling scans at the bottom) is only shown for the pure HEUR film, whereas the DSC heating curves of the nanocomposites are shown in **Fig. S2** in the Supporting Information (SI). The glass transition steps of all samples are shown in the inset in **Fig. 4**, and the values are reported in **Table 1**. No significant change in the glass transition temperature values (T_g) is observed with increasing MNP concentration. This refers to the glass transition temperature of the amorphous PEO portion. Looking at the heating curves on the top in **Fig. 4**, with increasing temperature, a double endotherm peak at $\sim -22\text{ }^\circ\text{C}$ may be discerned with peaks at $-27\text{ }^\circ\text{C}$ and at $-17\text{ }^\circ\text{C}$, the former one being more intense (indicated by the dashed line in **Fig. 4**).

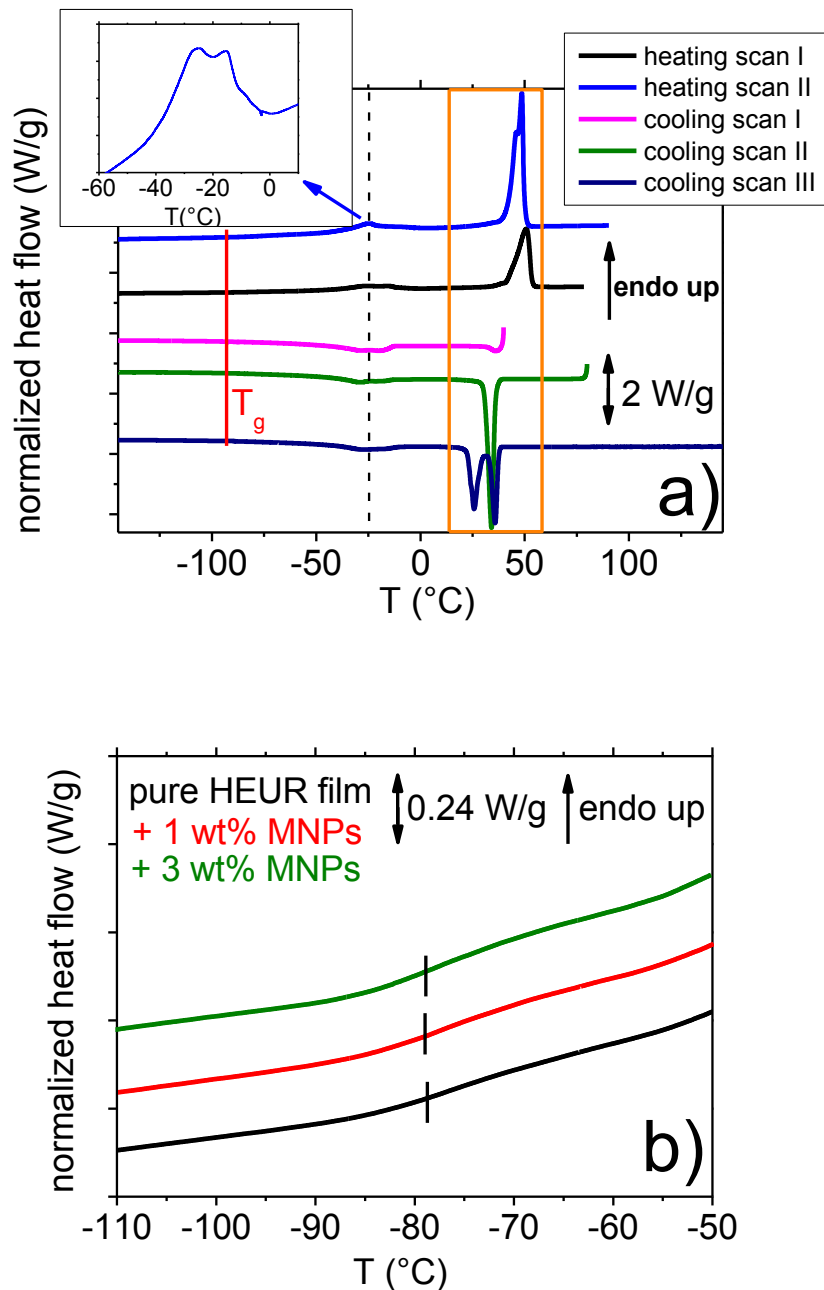


Fig. 4 a) DSC heating (scan I from -150 °C to 80 °C, scan II from -150 °C to 90 °C) and cooling curves (scan I from 40 °C to -150 °C, scan II from 80 °C to -150 °C, scan III from 150 °C to -150 °C) of the pure HEUR film with 10 °C/min. For clarity, the curves are shifted vertically. The dashed line indicates the melting/crystallization peak of the PEO crystallites at ~ -22 °C (the peak of the heating scan II is enlarged in the inset). The melting/crystallization peak of the crystalline PEO portion is highlighted by the orange rectangle. **b)** DSC heating thermograms showing the glass transition steps of the 3 nanocomposites. For clarity, the curves are shifted vertically. The glass transition temperatures T_g are calculated as the midpoint of the heat flow step and are indicated by short lines.

Sample	ΔH_m (J/g)	X_c	T_g (°C)	Δc_p (J/g °C)
Pure HEUR film	73.7± 2.2	0.37± 0.01	-79 ± 2	0.05± 0.01
+1 wt % MNPs	75.1± 2.3	0.38± 0.01	-78 ± 2	0.06± 0.01
+3 wt %MNPs	77.8± 2.3	0.39± 0.01	-80 ± 2	0.04± 0.01

Table 1 Enthalpy of melting ΔH_m , degree of crystallinity X_c , calorimetric T_g and heating capacities from DSC of the pure HEUR film and of the nanocomposites with 1 wt% MNPs and 3 wt% MNPs.

In previous calorimetric studies on polymer membranes containing water [22], a very similar endotherm transition was found in the same temperature range. According to previous studies, one might tentatively assign the more intense endotherm peak at lower temperature to the melting of the water clusters bound to the polymer chains and the second one at higher temperature to the “free” water molecules which are not directly bound to the polymer. From the water sorption measurements, we find that, in the relative humidity range rh of 40% and 80% (which can be defined as usual conditions), the investigated “dry” films contain a certain amount of water (h_d between 1% and 6%). Therefore, we might also ascribe the observed melting/crystallization peaks at ~ -22 °C to the water trapped in the polymer matrix.

However, in order to clarify whether the origin of this endothermic transition at ~ -22 °C is related to the water content, we acquired DSC cooling curves starting from three different temperatures, namely 40 °C, 80 °C and 150 °C (curves I,II and III shown at the bottom in **Fig. 4**). The aim of heating up to different temperatures prior to the run is to affect the state of the water absorbed in the film. Especially for scan III, the sample was heated up to 150 °C in order to be sure that any “clustered” water was fully evaporated.

In the cooling curves, the low temperature exotherm (corresponding to the “double” melting peak in heating) is located in all the scans in the temperature range between -40 °C

and -10 °C. The fact that these phase transitions appear similar in shape and that they occur at the same temperature in all scans, irrespectively of the water content, suggests that they are not related to the crystallization or melting of water. These crystallization/melting peaks may rather be attributed to the PEO chains, or PEO crystallites, that experience constraints different from the bulk PEO phase, leading to a remarkably strong suppression of crystallization. It is worth noticing at this point that, contrary to what would be expected in such systems, these crystallization (in the cooling scan) and melting (in the subsequent heating scan) peaks appear at the same temperature. Probably, the polyurethane (PU) segments interact with these PEO chains, leading to the observed thermal behavior. Due to the presence of these PEO crystallites, the system is quite heterogeneous.

The well-known and documented crystallization/melting of PEO [23] is observed in all scans in **Fig. 4** at ~50 °C (orange rectangle in **Fig. 4**) indicating that the HEUR polymer is, at least partially, crystalline. The degree of crystallinity of the polymer can be calculated by

$$X_c = \frac{\Delta H_{PEG}^*}{\Delta H_{PEG}^0} \quad (2)$$

Where ΔH_{PEG}^* is the enthalpy of fusion of the PEG portion of the HEUR polymer (0.095 kJ/g from the DSC curve) and ΔH_{PEG}^0 the enthalpy of fusion of 100% crystalline PEG ($\Delta H_{PEG}^0 = 0.19$ kJ/g) [24]. Similar DSC results were obtained for the nanocomposites (data shown in **Fig. S2** in the SI). The degree of crystallinity, X_c (with respect to the total polymer mass), and the enthalpy of melting, ΔH_m , of all investigated samples are listed in **Table 1** and demonstrate that the addition of MNPs only slightly affect the degree of crystallinity.

Also in the presence of the MNPs at concentrations of 1 wt% and 3 wt%, the crystallization/melting process of the small fraction of PEO displaying strong supercooling

is observed between -40 °C and -10 °C. Furthermore, the nanocomposites also show the crystallization/melting of the main crystalline PEO portion at ~ 50 °C and the glass transitions at $T_g \sim -75$ °C, as shown in **Fig. 4b**).

From the DSC measurements, we conclude that all the investigated systems are very heterogeneous. They consist of a main crystalline PEO portion, a small fraction of crystalline PEO which crystallizes/melts at lower temperature, and an amorphous part which gives rise to the observed glass transition. The MNPs do neither seem to affect the relative proportions of these phases nor their dynamics. This result is in agreement with the SANS data shown in our previous work [16]: The correlation peak at $q = 0.03 \text{ \AA}^{-1}$ which is related to the domain size of the polymer structure, i.e. the distance between the hydrophobic domains formed by the alkyl end groups of the HEUR polymer, does not shift with increasing MNP concentration. Therefore, neither the morphology of the sample nor its dynamics are affected by the presence of the MNPs.

3.3 Dynamic behavior in the temperature domain: Thermally stimulated depolarization current (TSDC) measurements

In order to investigate the dynamics of the systems under investigation in the temperature domain, TSDC measurements were performed. The thermograms of the pure HEUR film and of the nanocomposites at two different polarization temperatures, i.e. $T_p = 20$ °C and at $T_p = -60$ °C are shown in **Fig. 5**. At $T \sim 20$ °C, a very high depolarization current, I_n , is observed and reveals strong dc electrical conductivity for all the investigated samples. Besides the conductivity contribution, for all the samples, 2 dielectric dispersions are found. Starting from low temperatures, in the global TSDC thermograms obtained with $T_p = 20$ °C and $T_p = -60$ °C, we observe a peak (indicated by an arrow in **Fig. 5**) at ~ -75 °C for the pure HEUR sample and at ~ -79 °C and ~ -80 °C for both nanocomposites. This

dispersion is attributed to the so-called α -relaxation of the polymer, corresponding to the dynamic glass transition of the amorphous PEO, and its peak temperature is a good measure of the calorimetric T_g [25, 26].

In contrast to the TSDC results, no decrease of T_g with increasing MNP concentration is observed in the DSC data (**Fig. 4b**), but rather a step at $\sim -75^\circ\text{C}$ for all the samples. We

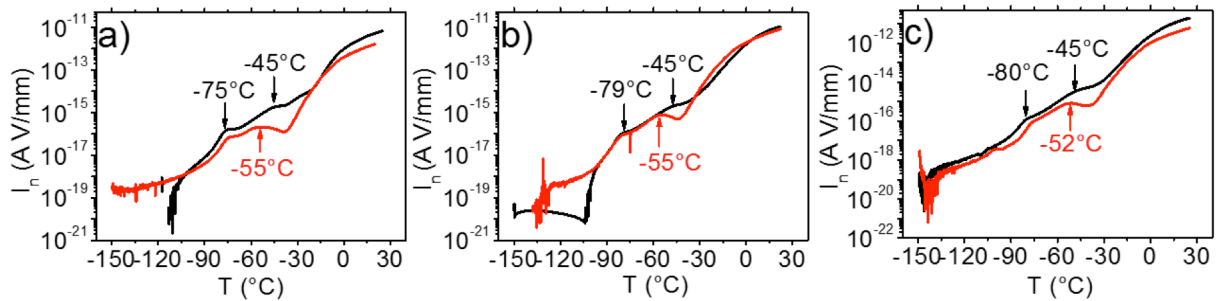


Fig. 5. TSDC thermograms of a) the pure HEUR film, b) the nanocomposites with 1 wt% MNPs and c) with 3 wt% MNPs polarized at $T_p = 20^\circ\text{C}$ (black curve) and at $T_p = -60^\circ\text{C}$ (red curve). The peak temperatures dispersions are annotated.

need to consider that the dispersion peak in the TSDC thermograms is affected by the depolarization current; thus, the observed decrease in the peak temperature cannot be attributed to a decrease in the glass transition of the amorphous PEO in a straightforward manner. At higher temperatures, an additional dispersion is observed with the peak temperature depending on the polarization temperature, T_p : It is located at $\sim -45^\circ\text{C}$ for $T_p = 20^\circ\text{C}$, and at $\sim -55^\circ\text{C}$ for $T_p = -60^\circ\text{C}$, indicated by the arrows in **Fig. 5**. The dependence of the position of this process on the polarization temperature implies that a charge polarization process may contribute to the electric dispersion. We also need to consider that the temperature at which this dispersions occurs corresponds to the onset of the

melting/crystallization process at ~ -40 °C, as detected in the DSC measurements (**Fig. 4a**). We remind here that we attributed this process to the melting/crystallization of strongly supercooled, small PEO crystallites that coexist with the main crystalline PEO phase and the amorphous PEO phase. Therefore, at this temperature, the sample is strongly heterogeneous. Thus, the detected dispersion at ~ -45 °C may be attributed to a dipolar-like process as the Maxwell-Wagner-Sillars (MWS) polarization which usually occurs in samples which are microphase-separated [27].

3.4 Dynamic behavior in the frequency domain: Dielectric relaxation spectroscopy (DRS) measurements

The dielectric relaxation spectroscopy measurements were performed in order to investigate the molecular dynamics of the systems. The dielectric loss spectra of the pure HEUR film at selected temperatures are shown in **Fig. 6** (the dielectric loss data of the nanocomposites are shown in **Figs. S3** and **S4** in the SI).

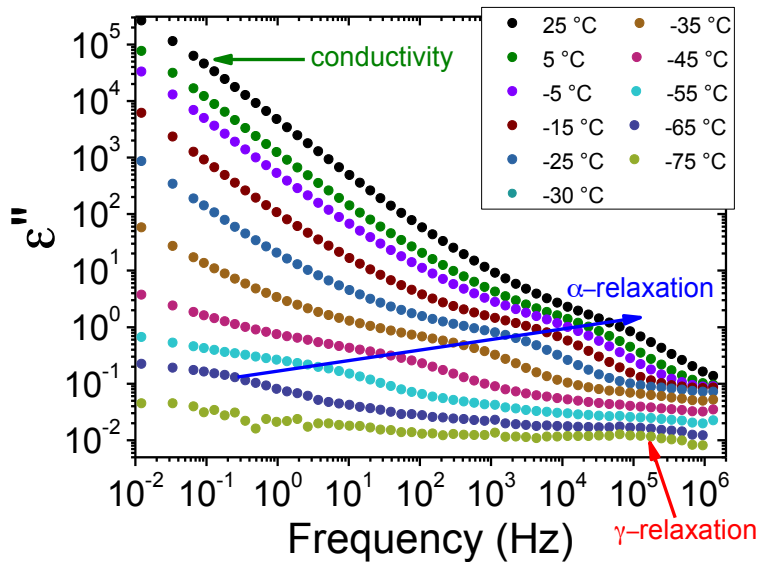


Fig. 6. Dielectric loss (ϵ'') data of the pure HEUR film. The blue arrow indicates the segmental relaxation of the polymer (α), the red one the secondary γ -process and the green one the conductivity contribution.

Following those spectra starting from low temperatures, we observe between -85°C and -45°C a weak relaxation process at frequencies of $\sim 10^5$ Hz. This process is attributed to the crankshaft motion of the methylene sequences in the PEO chain [28, 29], often termed as the γ -relaxation. At -65°C , a stronger relaxation enters the experimental window from the side of low frequencies. The α -relaxation in PEO has previously been observed at -50°C at 100 Hz [30]. Since the observed relaxation process is located in the same frequency range, we ascribe it to the α -relaxation of the amorphous PEO portions in the HEUR polymer, associated to its dynamic glass transition. At even lower frequencies (0.01 Hz – 1 Hz) and higher temperatures, a steep decay related to the DC-conductivity dominates the spectra, especially between -20°C and 25°C .

In the following, we will show that more relaxations coexist in the DC-conductivity dominated region. At this point, we would like to stress, that none of the 3 secondary relaxations, δ , γ and β that are typically observed in PU-based systems [31, 32] are found in the present systems. Instead, the dielectric spectra are dominated by the PEO contribution.

By comparing the dielectric loss data (ϵ'') of the 3 films with increasing MNP concentration at the same temperature, it is possible to observe differences in the dielectric behavior of the systems. For instance, in **Fig. 7**, we show the dielectric loss data of the 3 films at -45°C . It is possible to observe an increase of the imaginary permittivity ϵ'' in the low frequency range (0.01 Hz-1 Hz) as well as a moderate shift of the relaxation “shoulder” (black arrow in **Fig. 7**) to higher frequencies with increasing MNP concentration. This may be related to an acceleration of the segmental dynamics in the presence of nanoparticles, but may also just be an apparent acceleration due to the influence of the increased conductivity in the dielectric spectra of the nanocomposites.

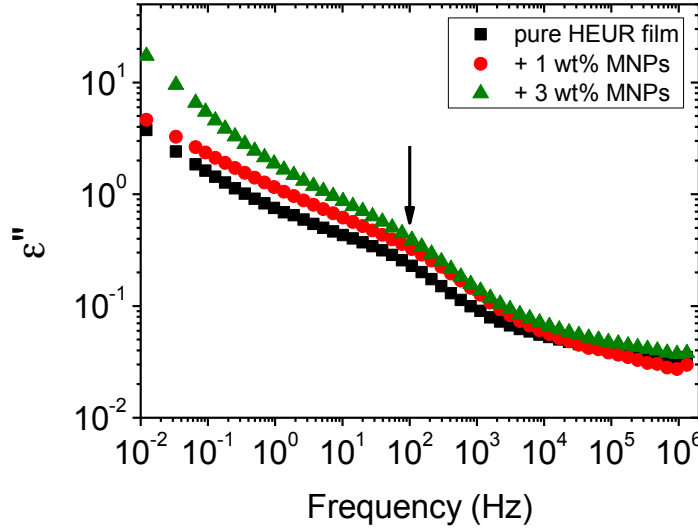


Fig. 7. Comparison of the dielectric loss data, ε'' , of the 3 samples with increasing MNP concentration at $-45\text{ }^{\circ}\text{C}$. The black arrow indicates the position of the shoulder related to the α -process.

3.4.1 Analysis of the DRS results

In order to quantify the effects on the segmental mobility and to investigate in detail the frequency region dominated by the conductivity, we performed an analysis based on fitting appropriate model functions. The dielectric loss spectra were fitted by a sum of Havriliak-Negami (HN) model function terms of the form:

$$\varepsilon^*(\omega) - \varepsilon_{\infty} = \frac{\Delta\varepsilon}{[1+(i\omega\tau_{HN})^{\alpha}]^{\beta}} \quad (3)$$

where $\tau_{HN}=1/\omega_{HN}$ is the characteristic relaxation time of each relaxation, $\Delta\varepsilon= \varepsilon_{\infty} - \varepsilon_0$ is the strength of the dielectric process, with ε_{∞} being the limit of the dielectric constant at high frequencies and ε_0 the vacuum permittivity, and the exponents α and β ($0 < \alpha, \beta < 1$) are

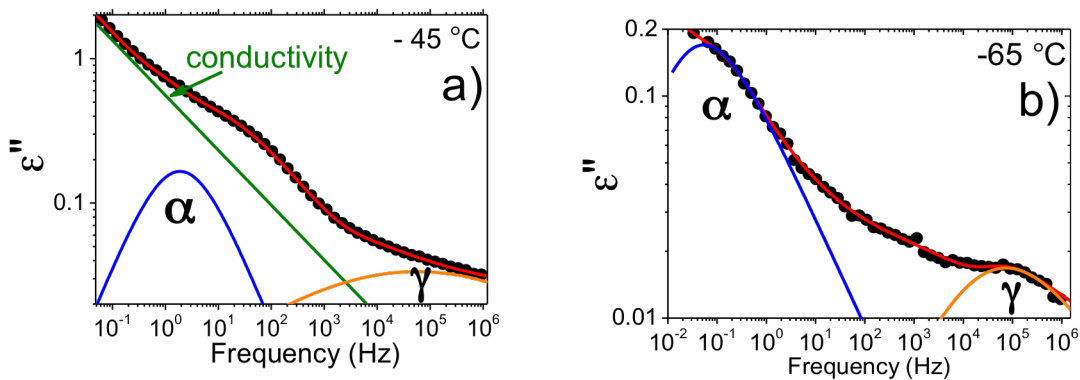
shape exponents, corresponding to the width and asymmetry of the peak, respectively. Values $\alpha = \beta = 1$ correspond to a single relaxation time causing a Debye peak.

From the data fitting, the relaxation time at the maximum of the processes, $\tau_{max} = 1/\omega_{max}$, is extracted as:

$$\omega_{max} = \omega_{HN} \frac{\sin\left[\frac{(1-\alpha)\pi}{2+2\beta}\right]^{1/(1-\alpha)}}{\sin\left[\frac{(1-\alpha)\beta\pi}{2+2\beta}\right]} \quad (4)$$

The effect of the conductivity in the temperature range between -80°C and 25°C was accounted for in the fit of the ε'' spectra by including a term of the form: $i\sigma/\omega^c \varepsilon_0$. with σ being the DC-conductivity of the material and c is an exponent with a value close to 1 [33, 34].

We fitted all the data by one relaxation process for the data collected between -35°C and 25°C and two relaxation processes for the data collected at lower temperatures, i.e. -45°C , -55°C and -65°C . Two examples of the fit with two relaxation processes at -45°C and at $-$



65°C for the pure HEUR film are shown in **Fig. 8**.

Fig. 8. Example of the fitting curves for the pure HEUR film at a) -45°C and b) -65°C . At -45°C , the contribution of the conductivity is shown. At -65°C , the contribution of the γ -relaxation is better visible (the contribution of the conductivity is not shown in order to emphasize the contributions of the relaxation processes).

Of particular interest are the results about the involved time scales, τ , which are given in an Arrhenius map in **Fig. 9**. For comparison, in the same plot, we also include the temperatures of the TSDC peaks, at the equivalent relaxation time of 100 s.

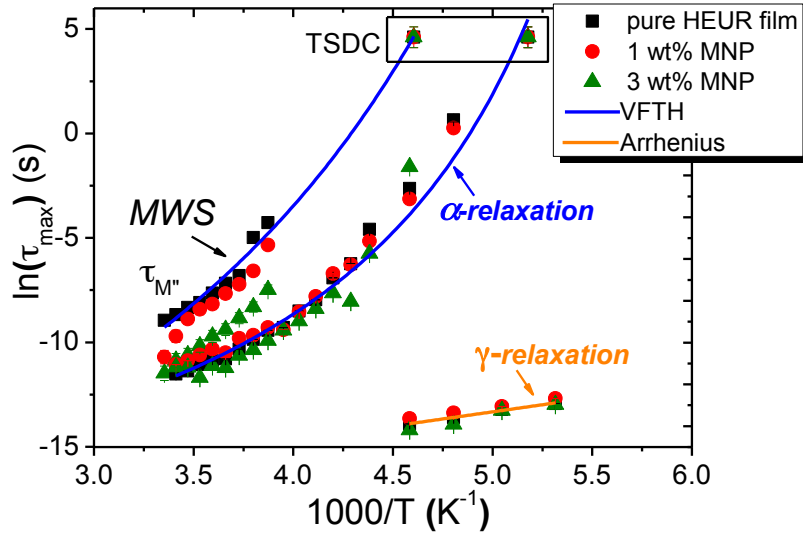


Fig. 9. Relaxation map showing the main processes and related fitting curves found for the 3 samples (pure HEUR polymer and nanocomposites), namely the VFTH-like polarization process (Mawell-Wagner-Sillars), the VFTH-like segmental relaxation (α) and the Arrhenius-like secondary relaxation (γ). $\tau_{M''}$ indicates that the relaxation times of the MWS polarization process are obtained from the M'' data (**Fig.10**). The details about the MWS process are discussed in the paragraph 3.4.2. Representative VFTH and Arrhenius fits are for the sample with 3 wt% are also shown. The dispersion peaks at -55 °C observed by TSDC are plotted at the equivalent relaxation time of 100 s.

The γ -relaxation follows an Arrhenius behavior:

$$\tau = \tau_0 e^{E_A/RT} \quad (5)$$

Where E_A is its activation energy. This confirms its local nature.

On the other hand, for all the samples, the main relaxation process occurring in the whole analyzed temperature range shows the Vogel-Fulcher-Tamman-Hesse (VFTH) temperature dependence:

$$\tau = \tau_0 e^{DT_0/(T-T_0)} \quad (6)$$

where τ_0 , D and T_0 are fitting parameters. The Vogel temperature T_0 is related to zero fraction of free volume of the cooperatively rearranging region. It is usually 30-40 °C below the glass transition temperature. This temperature dependence is typical of cooperative processes, i.e. the α -process (dynamic glass transition) [33].

In order to compare the DRS results with those from TSDC and DSC, we use the so-called dielectric glass transition temperature, $T_{g,diel}$. It is calculated by extrapolation of the VFTH fits (equation 6) to a standard relaxation time of 100 s. The glass transition temperatures T_g of the films are reported in **Table 2** and it is not affected by the MNP concentration in the polymer film. Therefore, we conclude that the presence of MNPs has no remarkable effect on the time scale of the main process in the nanocomposites. The glass transition temperatures calculated with equation 7 are within the uncertainties in agreement with the experimental values obtained by DSC.

MNP concentration (wt%)	$E_A(\gamma)$ (KJ/mol)	$T_{a,TSDC}$ (°C)	$T_{g,die}$ (°C)	D	τ_0 (ns)	T_0 (°C)
0	11.3 ± 0.7	-75 ± 5	-71.1 ± 1.2	3.3 ± 0.5	71 ± 3	-98.3 ± 1.6
1	11.1 ± 0.3	-80 ± 5	-71.5 ± 5.7	2.8 ± 0.6	250 ± 30	-97.4 ± 2.9
3	16.5 ± 0.9	-80 ± 5	-67.3 ± 7.1	1.5 ± 0.8	680 ± 90	-81.4 ± 6.7

Table 2. Activation energies E_A related to the γ -process, T_a from TSDC, $T_{g,die}$ calculated from the VFT fits, and the parameters used in the VFTH fits of the α -relaxation.

A difference in the VFTH fits is revealed by the limiting values of the relaxation time for infinite temperature, τ_0 (**Table 2**). It increases with increasing the MNP concentration. The quantity τ_0 is usually assumed to be equal to a typical phonon frequency, which is of the order of 2-10 THz [33]. Deviations from the expected range of τ_0 can be explained by a transition to a different temperature dependence at very high temperatures. Another interesting difference in the relaxation map regards the γ -relaxation detected at low temperatures [35]. Despite the limited number of experimental points related to the γ -relaxation, we fit them using the Arrhenius equation (eq. 5), and obtained the activation energy values $E_A(\gamma)$ reported in **Table 2**. The results suggest a slightly elevated activation energy for the nanocomposite with 3 wt% MNP concentration. We believe that this effect might be related to the changes in nano-morphology as demonstrated by the slight increase of the degree of crystallinity (**Table 1**) and the changes in the degree of microphase separation [16]. The methylene sequences, whose crankshaft motion gives rise to the γ -relaxation, are expected to face in the interfaces different energy landscapes that inhibit slightly their mobility. The same kind of effects on the activation energy of the γ -relaxation, was observed in PU systems [36]. In general, the relaxation map shows no big difference between the dynamics of the pure HEUR film and the nanocomposites, meaning that the MNPs do not seem to influence the dynamics of the HEUR polymer. This is most

probably due to the fact that the MNPs, being coated with oleic acid and oleylamine, interact mainly with the hydrophobic ends of the telechelic HEUR polymer. Therefore, they do not influence the motions associated to the main PEO (polar) chain. This result is in agreement with the structural characterization previously performed by SANS measurements [16] in which we did not observe any influence of the MNPs on the domain spacing of the polymer matrix. Therefore, the MNPs addition neither affects the structure nor the dynamics of the polymer matrix. This means that the morphology is not modified and that the fragility of the material is not increased upon the addition of MNPs. However, as detailed below, the MNPs have an effect on the conductive behavior of the materials.

3.4.2 High conductivity region – charge transport effects

In the following section, the details about the MWS relaxation are discussed. Increasing the temperature to the range -20 °C to 25 °C, a very high conductivity contribution is observed in the low frequency region. This region, however, cannot be fitted adequately by a simple DC-conductivity process. In addition, following the results by TSDC, one more relaxation is expected in this temperature range. For conductive systems, it is advantageous to describe the conduction mechanism using the formalism of the electrical modulus $M^*(\omega) = 1/\varepsilon^*(\omega)$ [37, 38]. In the following, by comparing different formalisms for the description of the dielectric response, we will try to extract information on the underlying mechanisms.

In **Fig. 10**, the dielectric loss data of the pure HEUR film at 10 °C are shown together with the corresponding $M''(\omega)$ data. They exhibit a low-frequency peak, highlighted in **Fig. 10** with a magenta arrow. The peak at higher frequency (indicated by the blue arrow) is

attributed to the segmental relaxation associated with the glass transition of the amorphous PEO, i.e. the α -relaxation.

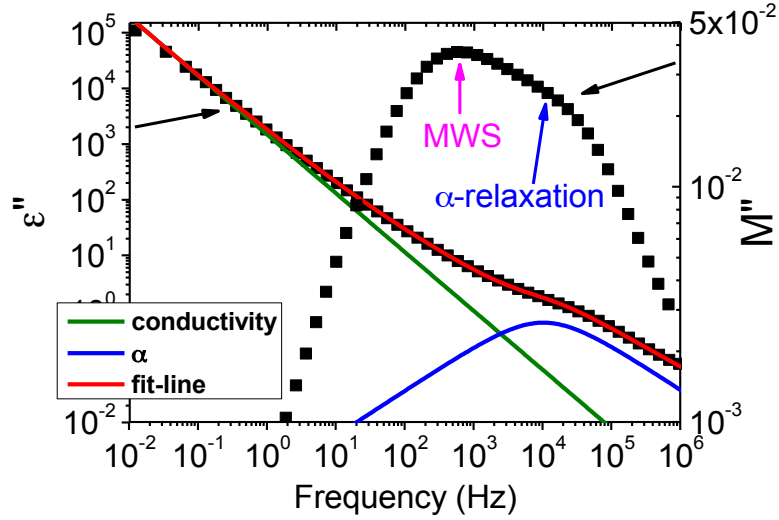


Fig. 10. Example of the fitting curve (at 10 °C) used for the dielectric loss data of the pure HEUR film in the temperature range between -15 °C and 25 °C. The corresponding data in the modulus representation are shown, and the assigned relaxation processes are highlighted (see text).

In **Fig. 11**, we show the $M''(\omega)$ curves at 4 different temperatures, namely 20 °C, 5 °C, -10 °C and -20 °C, where we observe very high conductivity in the corresponding dielectric loss data. It is known that the $M''(\omega)$ curves should exhibit low frequency peaks at frequency ω_{max} , at the crossover frequency of the corresponding conductivity data, $\sigma'(\omega)$. The crossover frequency in the conductivity data is the frequency value where the $\sigma'(\omega)$ curves start to change from the dc plateau values at lower frequencies to the power law dependence at higher frequencies [39]. We compare the $M''(\omega)$ curves with the conductivity data $\sigma'(\omega)$ in **Fig. 11**, and the crossover frequency is highlighted in the conductivity data. The expected peak at such crossover frequencies in the electrical modulus formalism are the manifestation of the so-called conductivity relaxation [37]. However, in the case of the pure HEUR film we note that, except for the data at -20°C, the maximum frequency of the low-frequency peak in the $M''(\omega)$ is located at higher

frequency than the crossover of the conductivity data (see dashed lines in **Fig.11**). For the nanocomposites, we observe the same “shift” of ω_{max} of the low frequency peak in the $M''(\omega)$ curves to a higher frequency than the crossover frequency in the $\sigma'(\omega)$ curves, also at -20°C . In this case, the peak at low frequency in the modulus formalism is not very well separated from the one related to the α -process, as it is for the pure HEUR film.

This result suggests that another process occurs in the low frequency region in addition to the conductivity relaxation. This process is most probably due to an interfacial polarization mechanism, because of the low frequency region of occurrence (10^{-1} -10 Hz), probably of the type of the Maxwell-Wagner-Sillars (MWS) which occurs typically in systems comprised of regions with different conductivities [27].

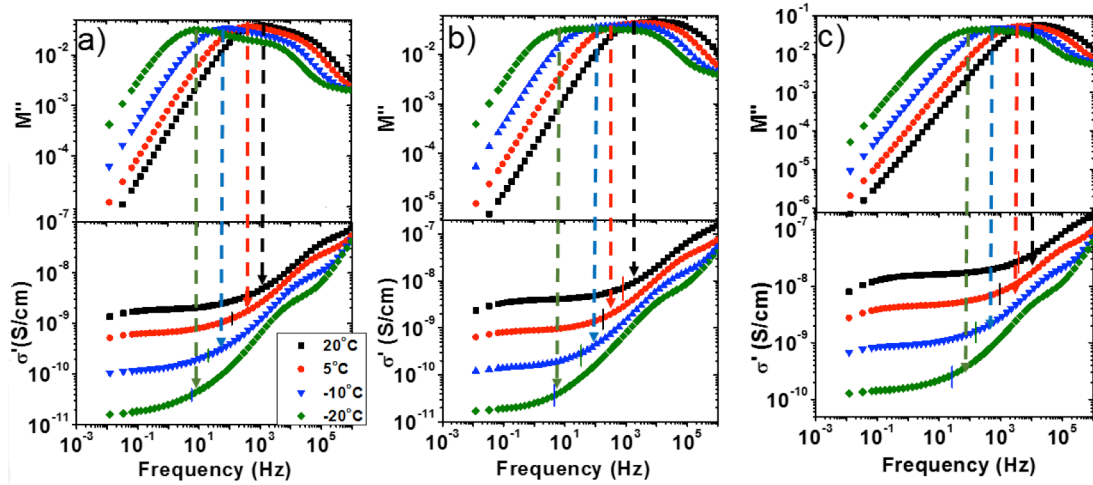


Fig. 11. Real part of the conductivity σ' and imaginary part of the modulus M'' as a function of the frequency of a) the pure HEUR film, b) with 1 wt% MNPs and c) with 3 wt% MNPs at 4 different temperatures (20°C , 5°C , -10°C , -20°C). The dashed arrows connect the maxima of the $M''(\omega)$ curves at low frequency with the crossover frequency in the conductivity data which are marked by short vertical lines.

Additional information about the processes occurring in the low frequency region in the temperature range between -20°C and 25°C can be extracted from the first derivative of the real part of the dielectric permittivity $\varepsilon''_{der} = \delta\varepsilon'/\delta\ln\omega$. The ε''_{der} data turn out to be useful for systems which exhibit low-frequency relaxations alongside an appreciable Ohmic conductivity [40], as the $\varepsilon'(\omega)$ values are in principle not affected by the Ohmic conductivity, and according to the Kramers-Kronig relationships, its derivative is proportional to the part of $\varepsilon''(\omega)$ which arises from dipolar processes. Indeed, in the derivative formalism, the relaxation processes visible in the dielectric loss data appear as sharper peaks and without the conductivity contribution [41]. In **Fig. 12**, we compare the dielectric loss data ε'' and the corresponding derivative data $\delta\varepsilon'/\delta\ln\omega$ at 20°C for the pure HEUR film (the data of the nanocomposites show identical results).

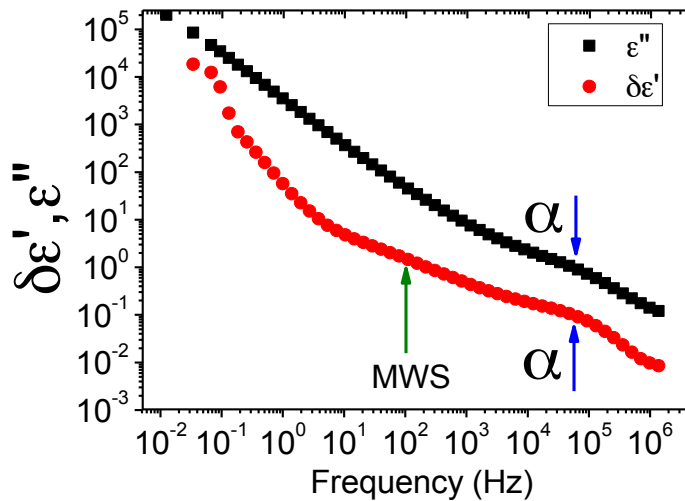


Fig.12 Dielectric loss data ε'' (black squares) and derivative of the real part of the permittivity $\delta\varepsilon'$ (red squares) at 20°C for the pure HEUR film. The processes detected in the derivative data (the α -process and the MWS polarization process) are highlighted by the arrows.

From the derivative $\varepsilon''_{der} = \delta\varepsilon'/\delta\ln\omega$ data, we identify three processes. The one occurring at high frequencies ($\sim 10^5$ Hz) is the α -relaxation of the polymer as observed earlier in the

conventional dielectric loss data. At low frequencies, we observe two shoulders which are not visible in the ϵ'' formalism, namely at $\sim 10^{-1}$ Hz and at ~ 70 Hz, respectively (highlighted by a green arrow in **Fig. 12**). The origin of the process at $\sim 10^{-1}$ Hz is not yet completely understood. In the TSDC measurements, we observed a dispersion depending on the polarization temperature at $T \sim -45$ °C and at $T \sim -55$ °C at low frequency ($\sim 10^{-1}$ Hz), which originates from a charge polarization process. The low-frequency processes observed in the modulus and in the derivative formalisms can be associated to the dispersion found in TSDC. Thus, they could originate from a polarization mechanism, most likely of the type of MWS, since it usually reflects a microphase separation within the sample [42, 43]. According to previous small angle neutron scattering data of the investigated HEUR polymer-based nanocomposites [16], indeed, a microphase separation is observed. It originates from the phase separation between the hydrophobic domains (composed of the alkyl ends of the HEUR telechelic polymer) and the hydrophilic backbone of the polymer chain, mainly composed of PEO. The addition of the MNPs up to 3 wt% leads to the formation of clusters of MNPs. On the other hand, according to the DSC and TSDC measurements, the pure HEUR film, as well as the nanocomposites, are characterized by high heterogeneity mainly caused by the PEO portion which is present in three phases: (i) the amorphous PEO, giving rise to the glass transition at ~ -75 °C, (ii) small crystalline PEO regions where strong confinement of the PEO chains occurs and (iii) the main crystalline PEO phase which gives rise to the melting process at ~ 50 °C. Therefore, we tend to attribute the MWS interfacial polarization process, which contributes to the detected low-frequency dispersions, to the heterogeneity of the PEO domains.

The dispersion process observed in the TSDC data at -55 °C, which we assigned to the MWS polarization process (**Fig. 5**), most likely corresponds to the relaxation process

detected in the derivative of the real part of the permittivity ε''_{der} at $\sim 10^2$ Hz (indicated by the green arrow in **Fig. 12**). We do this assignment also taking into account the frequency where the peak at low frequency occurs in the modulus representation (**Fig. 10**, magenta arrow), which is at $f_{max} \sim 600$ Hz. In fact, the ω_{max} values of the relaxation processes detected in the modulus representation are shifted to higher frequencies than in the permittivity formalism [33]. In the Arrhenius plot presented in **Fig. 9**, we included the M'' peak frequencies of the slower component of the composite peak which corresponds to this low frequency peak in ε''_{der} . Its trace follows a VFTH temperature dependence and agrees well with the peaks observed with TSDC around -55°C . This implies that the dispersion observed in the TSDC data corresponds to the same mechanism as the one detected in the DRS data in the temperature range between -20°C and 25°C .

The origin of the smaller relaxation at $\sim 10^{-1}$ Hz is yet unclear, however it may be related to slower dynamics of PEO at the interfaces between amorphous and crystalline domains (the so called α') or in amorphous areas inside the crystallites (the so-called α_C) [44-46].

3.4.3 Comparison of the conductivity data of the pure HEUR film and the nanocomposites – polymer conductivity effect

In the high temperature region of the Arrhenius map shown in **Fig.9**, it is possible to observe a faster dynamics for the nanocomposite with 3 wt% MNPs. In fact, the relaxation times $\tau_{M''}$ associated to the interfacial polarization mechanism (MWS-relaxation) are smaller than those of the other two samples. This effect on the relaxation times $\tau_{M''}$ of the MWS relaxation can be explained by considering the proportionality between the relaxation time and the conductivity, σ' , of the material. In particular, the relaxation time is known to be inversely proportional to the conductivity of the sample [33]. Indeed, looking at the conductivity data, σ' , at -10°C shown in **Fig. 13**, we may observe that the plateau of

the conductivity profile is one order of magnitude higher for the sample with the 3 wt% MNPs than for the other two samples.

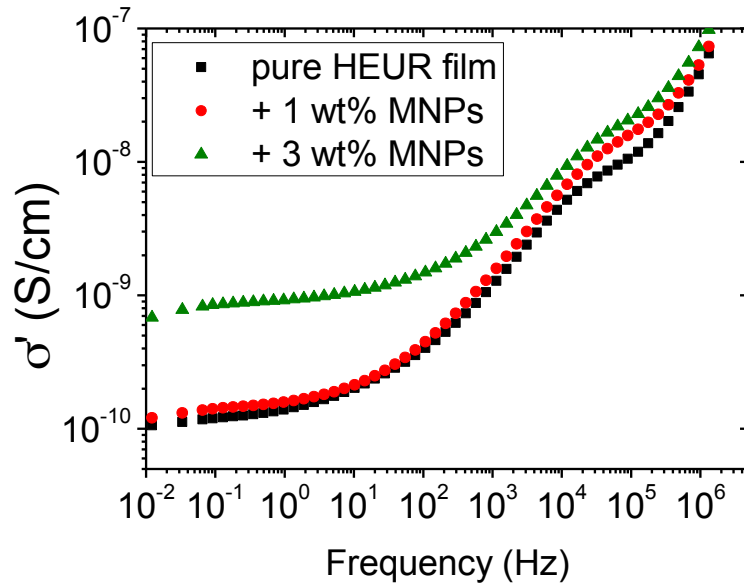


Fig.13 Conductivity data σ' (S/cm) of all the investigated samples at -10 °C.

The increase of the conductivity for the nanocomposite containing 3 wt% MNPs, is reflected also in the increase of the permittivity value, ϵ'' , as seen in **Fig. 7**.

In order to understand the origin of such a steep increase of the conductivity upon an increase of the MNP concentration to 3 wt%, we constructed the Arrhenius plot for the conductivity by plotting the conductivity plateau values as a function of inverse temperature (**Fig. 14**). The Arrhenius plot gives information about the conductivity mechanism occurring in the samples. However, as shown in **Fig. 14**, for all the samples, the conductivity shows the same kind of temperature dependence, i.e. a VFTH-like, with only small differences in the curves. Therefore, the conductive mechanism occurring in the films must be the same for all the samples.

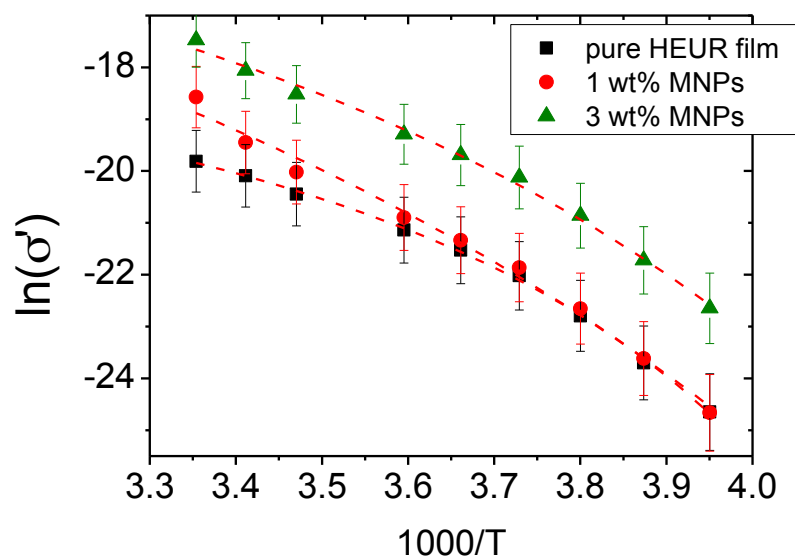


Fig. 14 Arrhenius map of the conductivity for all the samples. The dashed lines are guides for the eyes.

The fact that, upon addition of MNPs, we observe the same kind of conductive mechanism as in the pure HEUR film, implies that the MNPs affect only indirectly the conductive phase of the film, which is the amorphous PEO phase. In the structural characterization of the nanocomposites [16], we observed the formation of large clusters of MNPs at an MNP concentration of 3 wt% (**Fig. 15**). However, single MNPs coexist with the MNPs clusters in the final nanocomposite formulation (**Fig.15 b**)), indicating that the HEUR polymers partially disperse the hydrophobic MNPs. As observed in our previous work on the dynamics of HEUR hydrogel network with embedded MNPs [47], the presence of the MNPs clusters close to the hydrophobic domains of the network leads to a “dilution” of the polymers near the hydrophobic domains, allowing a higher mobility of the polymer backbone. Indeed, in presence of the big clusters of MNPs, the hydrophobic domains become larger, leading to a considerably different grafting of the sticky hydrophobic ends of the polymer on the hydrophobic domains. This gives more space to the amorphous PEO to re-arrange. We believe that we observe the same effect in the dry films, thus, the higher

degrees of freedom gained by the amorphous PEO allows an easier charge transport, leading to the observed increase of the conductivity.

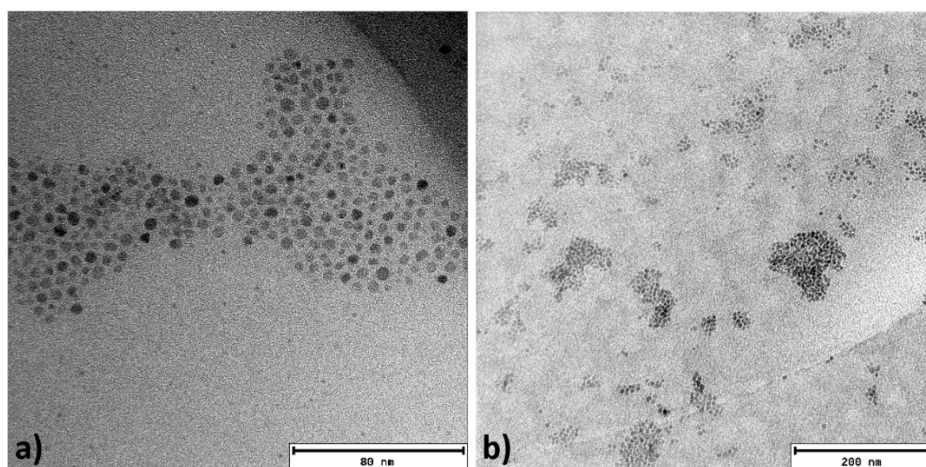


Fig.15 TEM image of the HEUR dry film with a concentration of MNPs of 3 wt% showing **a)** large cluster of MNPs and **b)** large clusters of MNPs coexisting with single MNPs, indicating that the HEUR polymer matrix partially disperses the MNPs

4. Summary and conclusions

The dynamics and the thermal behavior of nanocomposites composed of HEUR polymer and coated magnetite nanoparticles are investigated with DSC, TSDC and DRS measurements. Nanocomposites as dry films are studied and are compared with a pure HEUR film which serves as a reference. The thermal behavior is investigated using DSC, and three main phase transitions are detected, revealing a high heterogeneity for all the investigated samples: (i) the glass transition of the amorphous PEO portion at ~ -75 °C, (ii) the crystallization/melting between ~ -40 °C and ~ -10 °C of the PEO crystallites which experience different constraints as compared with the PEO bulk phase, and (iii) the crystallization/melting at ~ 50 °C of the crystalline PEO phase. The pure HEUR sample is

found to be semi-crystalline with a degree of crystallinity of 37 % with a water content of 6 % (at relative humidity $rh = 80\%$).

The dynamics of all samples are investigated by employing TSDC and DRS methods. TSDC measurements, directly related with DSC experimental findings, reveal the existence of two main dispersions. The one at ~ -75 °C, which does not depend on the polarization temperature, T_p , is attributed to the segmental relaxation of the amorphous portion of PEO (α -relaxation). The second dispersion observed at higher temperature, namely at ~ -5 °C, has been found to depend on T_p , meaning that a dipolar-like mechanism, like the Maxwell-Wagner-Sillars (MWS) polarization process may be involved. The MWS process is usually observed when the sample is microphase-separated. Because of the high heterogeneity of the investigated samples detected previously [16], this was expected. Finally, the TSDC measurements revealed a strong DC electrical conductivity at $T \sim 20$ °C. The contribution of the high DC electrical conductivity is visible also in the DRS data, especially in the temperature range between -20 °C and 25 °C, giving rise to a very high imaginary permittivity, ϵ'' , at low frequency. Because of this strong DC-conductivity contribution, the analysis of processes occurring in the low-frequency range is carried out considering the electrical modulus and the derivative formalisms. The $M''(\omega)$ curves reveal the contribution of additional low-frequency processes to the conductivity relaxation. Two low-frequency processes, not visible in the dielectric loss data, ϵ'' , are detected also in the derivative of the real part of the permittivity, ϵ' . These results confirm the occurrence of the low-frequency processes revealed by TSDC, and show that they are probably due to a polarization mechanism, like the MWS polarization, which is characteristic of heterogeneous systems. From the dielectric measurements, three relaxation processes are detected: (i) at -20 °C $< T < 25$ °C, a low-frequency process, which we suggest to be related to the MWS polarization; (ii) at -65 °C $< T < 25$ °C the α -process associated to the

dynamic glass transition of the amorphous PEO; and (iii) at $T < -55$ °C, the γ -process, attributed to the crankshaft motion of the methylene groups.

No influence of the addition of MNPs to the pure HEUR film on the α -relaxation of the HEUR polymer was observed. This means that structural properties of the material, such as the glass transition T_g and its fragility, are not affected by the presence of the MNPs. This result is in agreement with the structural characterization of the nanocomposites, which revealed no change in the domain spacing of the polymer network with increasing concentration of MNPs [16]. We believe that the MNPs do not influence the α -relaxation of the HEUR polymer because, being coating with an hydrophobic shell, they interact mainly with the its hydrophobic ends and not with the amorphous PEO portion, Therefore, the change of polarity of the MNPs coating could probably lead to stronger interactions with the PEO chains, resulting in a modification of the dynamics of the nanocomposites compared to the pure HEUR film. On the other hand, the addition of MNPs influences the γ -relaxation at low temperatures. In particular, we observe an increase of its activation energy $E_A(\gamma)$ for the nanocomposite with 3 wt% MNP concentration. We ascribe this effect to the slight increase of the crystallinity degree of the PEO portion (**Table 1**) upon increasing the MNP concentration. We believe that the increase of the crystallites size inhibits the crankshaft motion of the methylene sequences of the polymer backbone.

Finally, we observe a steep increase of the DC-conductivity in the temperature range between -20 °C and 25 °C upon increasing MNP concentration. We ascribe this increase to the formation of large clusters of MNPs (**Fig. 15**) which leads to a lower “grafting density” of the hydrophobic ends of the HEUR polymer than in the case of the pure film (characterized by smaller hydrophobic domains). The lower polymer concentration near the clusters allows the polymer to re-arrange more easily, thus, promoting the charge transport. This effect leads to an increase of the conductivity of the system. [Despite the not](#)

perfect MNPs dispersion into the polymer matrix, as visible in **Fig.15**, we manage to achieve two main results upon the addition of MNPs : the increase of the conductivity and the keeping of the glass transition temperature. The combination of these features allows the use of these nanocomposites for applications that require high conductivity without increasing the fragility of the material.

Acknowledgements

Prof. Müller-Buschbaum acknowledges funding by the Nanosystems Initiative Munich (NIM). We thank Dr. Sotiria Kriptomou (NTUA, Athens) for her assistance with the water sorption, calorimetric and especially the thermally stimulated depolarization current (TSDC) measurements.

References

- [1] S. Kalia, S. Kango, A. Kumar, Y. Halsorai, B. Kumari, R. Kumar, *Colloid Polym. Sci.*, 2014, 292, 2025
- [2] H. Gu, P.L. Ho, K. W. T. Tsang, L. Wang, B. Xu, *J. Am. Chem. Soc.* 2003, 125, 15702-15703.
- [3] Y.Yao, E.Metwalli, B.Su, V.Körstgens, D.Moseguí González, A.Miasnikova, A.Laschewsky, M.Opel, G.Santoro, S.V.Roth, P.Müller-Buschbaum, *ACS Appl. Mater. Interfaces*, 2015, 7, 13080-13091
- [4] Q. Wei, Y. Lin, E. R. Anderson, A.L. Briseno, S. P. Gido, J. J. Watkins, *ACS Nano* 2012, 6, 1188-1194.
- [5] Y. Yao, E. Metwalli, M. A. Niedermeier, M. Opel, C. Lin, J. Ning, J. Perlich, S.V. Roth, P. Müller-Buschbaum, *ACS Appl. Mater. Interfaces*, 2014, 6, 5244-5254

- [6] A. C. Balazs, T. Emrick, T. P. Russell, *Science* 2006, 314, 1107-1110.
- [7] I. Kong, S.H. Ahmad, M. H. Abdullah, D. Hui, A. N. Yusoff, D. Puryanti, *J Magnetism and Magnetic Materials*, 2010, 322, 3401–3409
- [8] Bregar V.B., *IEE Tran on Magn*, 2004, 40, 3, 1679-1684
- [9] A.-H. Lu, E. L. Salabas, F. Schüth, *Angew. Chem., Int. Ed.* 2007, 46, 1222-1244.
- [10] G. Kortaberria, P. Arruti, I. Mondragon, L. Vescovo, M. Sangermano, *J. Appl. Polym. Sci.*, 2011, 120, 2361-2367.
- [11] V. Lauter-Pasyuk, H. Lauter, G. Gordeev, P. Müller-Buschbaum, B. Toperverg, M. Jernenkoy, W. Petry, *Langmuir*, 2003, 19, 7783-7788.
- [12] Y. Lin, A. Böker, J. He, K. Sill, H. Xiang, C. Abetz, X. Li, J. Wang, T. Emrick, S. Long, Q. Wang, A. Balazs, T. P. Russell, *Nature*, 2005, 434, 55-59.
- [13] M. M. Abul Kashem, J. Perlich, A. Diethert, W. Wang, M. Memesa, J. S. Gutmann, E. Majkova, I.c. Capek, S. V. Roth, W. Petry, P. Müller-Buschbaum, *Macromolecules* 2009, 42, 6202-6208.
- [14] X. Xia, E. Metwalli, M. A. Ruderer, V. Körstgens, P. Busch, P. Böni, P. Müller-Buschbaum, *J. Phys.: Cond. Mat.* 2011, 23, 254203.
- [15] K. Aissou, T. Alnasser, G. Pecastaings, G. Goglio, O. Toulemonde, S. Mornet, G. Fleury, G. Hadziioannou, *J. Mater. Chem.* 2013, 1, 1317-1321.
- [16] A. Campanella, Z. Di, A. Luchini, L. Paduano, A. Klapper, M. Herlitschke, O. Petravic, M.S. Appavou, P. Müller-Buschbaum, H. Frielingaus, D. Richter, *Polymer*, 2015, 60, 176-185
- [17] L Wang., J. Luo, Q. Fan, M. Suzuki, I.S. Suzuki, M.H. Engelhard, Y. Lin, N. Kim, J.Q. Wang, C.J. Zhong, *J. Phys. Chem. B*, 2005, 109, 21593-21601
- [18] H. Engels, H.G. Pirkel, R. Albers, R.W. Albach, J. Krause, A. Hoffman, H. Casselmann, J. Dormish, *Angewandte Chemie*, 2013, 52, 9422-9441
- [19] F. Kremer, *J Non-Cryst Solids*, 2002, 305, 1–9
- [20] J. van Turnhout, in: G. M. Sessler (Ed.) *Electrets. Topics in Applied Physics*, Vol. 33 (Springer, Berlin, 1980), 81-215

- [21] C. Pandis, A. Spanoudaki, A. Kyritsis, P. Pissis J.C. Rodriguez Hernandez, J.L. Gomez Ribellez M. Monleon Pradas. *J. Polym. Sci. B Polym. Phys.*, 2011, 49, 199-209
- [22] Shimadzu, 2015, Retrieved from
<http://www.shimadzu.com/an/industry/electronicselectronic/fc160306010.htm>
- [23] K. Pielichowski, K. Fleituch, *Polym. Adv. Technol.*, 2002, 13, 690-696
- [24] A. Bartolotta, G. Di Marco, M. Lanza, G. Carini, *Il Nuovo Cimento*, 1994, 16, 825-830
- [25] Martuscelli, E., Silvestre, C., Gismondi, C., *Die Makromolekulare Chemie*, 1985, 186, 2161-2176
- [26] Connor, T. M.; Read, B. E.; Williams, G., *J Appl Chem*, 1964, 14, 74
- [27] R.W. Sillars, *J Inst Electr Engin*, 1937, 80, 378-394
- [28] A. Kyritsis and P. Pissis, *J. Polym. Sci., Polym. Phys. Ed.*, 1997, 35, 1545 - 1560
- [29] X. Jin, S. Zhang, J. Runt, *Polymer*, 2002, 43, 6247-6254
- [30] J.J. Fontanella, M.C. Wintersgill, P.J. Welcher, J.P. Calame, *IEEE Tran on Electrical insulation*, 1985, 6, 943-946
- [31] D. S. Huh, S. L. Cooper, *Polym Eng Sci*, 1971, 11, 369-376
- [32] P. Ortiz-Serna, M. Carsí, B. Redondo-Foj, M. J. Sanchis, M. Culebras, C. M. Gómez, A. Cantarero, *J Appl Polym Sci*, 2015, 132, 42007 (1-8)
- [33] F. Kremer, A. Schönhals, *Broadband Dielectric Spectroscopy*, 2003, Berlin, Springer-Verlag Berlin Heidelberg
- [34] N.G. McCrum, B.E. Read, G. Williams, *Anelastic and Dielectric Effects in Polymer Solids*, 1967, New York, Dover
- [35] J. C. Mauro, Y. Yue, A. J. Ellison, P. K. Gupta, and D. C. Allan, *Proc. Nat. Acad. Sci. USA*, 106, 19780 (2009).
- [36] K.N. Raftopoulos, B. Janowski, L. Apekis, K. Pielichowski, P. Pissis, *Eur Polym J*, 2011, 47, 2120–2133
- [37] P.B. Macedo, C.T. Moynihan, R. Bose, *Phys Chem Glasses* 1972, 13, 171-179

- [38] A. Kyritsis, P. Pissis, J. Grammatikakis, *J Polymer Sci : Part B: Polymer Physics*, 1995, 33, 1737-1750
- [39] A. Kyritsis, K. N. Raftopoulos, M.A. Rehim, S.S. Shabaan, A. Ghoneim, G. Turky, *Polymer*, 2009, 50, 4039-4047
- [40] M. Wübbenhorst, J. van Turnhout, *J Non-Cryst Solids*, , 2002, 305, 40-49
- [41] M. Wübbenhorst, E. van Koten, J.Jansen, W. Mijs, J. Van Turnhout, *Macromolecules Rapid commun.*, 1997, 18, 139
- [42] K.N. Raftopoulos, S. Koutsoumpis, M. Jancia, J.P. Lewicki, K. Kyriakos, H.E. Mason, S.J. Harley, E. Hebda, C.M. Papadakis, K. Pielichowski, P. Pissis, *Macromolecules*, 2015, 48, 1429-1441
- [43] A.S. Vatalis, A. Kanapitsas, C. G. Delides, K. Viras, P. Pissis, *Thermochimica Acta*, 2001, 372, 33-38
- [44] K. Se, K. Adachi, T. Kotaka, *Polymer Journal*, 1981, 13, 1009-1017
- [45] M. Takayanagi, *Proceedings of the Fourth International Congress of Rheology*, Vol.1, E.H. Lee, Ed. Providence, Rhode Island, 1963, p 161
- [46] Y. Ishida, *J. Polym. Sci.*, 1969, 7, 1835
- [47] A. Campanella, O. Holderer, K. N. Raftopoulos, C. M. Papadakis, M. P. Staropoli, M. S. Appavou, P. Müller-Buschbaum, H. Frielinghaus, *Soft Matter*, 2016, Advance Article, doi:10.1039/C6SM00074F.